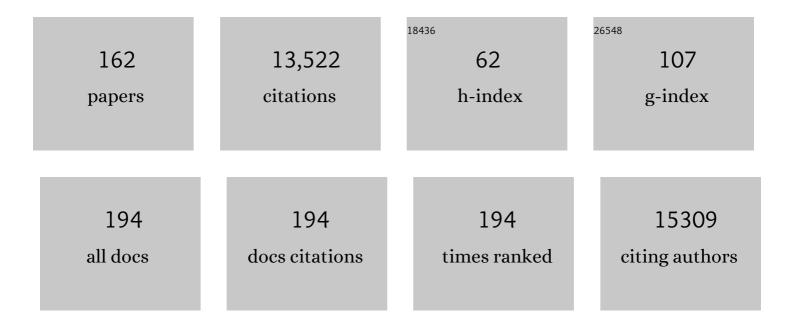
Sriram Subramaniam

List of Publications by Year in descending order

Source: https://exaly.com/author-pdf/9207310/publications.pdf Version: 2024-02-01



#	Article	IF	CITATIONS
1	A paradigm shift in structural biology. Nature Methods, 2022, 19, 20-23.	9.0	27
2	SARS-CoV-2 Omicron variant: Antibody evasion and cryo-EM structure of spike protein–ACE2 complex. Science, 2022, 375, 760-764.	6.0	488
3	Structural and biochemical rationale for enhanced spike protein fitness in delta and kappa SARS-CoV-2 variants. Nature Communications, 2022, 13, 742.	5.8	71
4	Comparison of side-chain dispersion in protein structures determined by cryo-EM and X-ray crystallography. IUCrJ, 2022, 9, 98-103.	1.0	4
5	Malaria parasites use a soluble RhopH complex for erythrocyte invasion and an integral form for nutrient uptake. ELife, 2021, 10, .	2.8	35
6	Cryo-electron microscopy structures of the N501Y SARS-CoV-2 spike protein in complex with ACE2 and 2 potent neutralizing antibodies. PLoS Biology, 2021, 19, e3001237.	2.6	171
7	Glycan reactive anti-HIV-1 antibodies bind the SARS-CoV-2 spike protein but do not block viral entry. Scientific Reports, 2021, 11, 12448.	1.6	22
8	AAA+ ATPase p97/VCP mutants and inhibitor binding disrupt inter-domain coupling and subsequent allosteric activation. Journal of Biological Chemistry, 2021, 297, 101187.	1.6	13
9	New insights into Raf regulation from structural analyses. Current Opinion in Structural Biology, 2021, 71, 223-231.	2.6	4
10	A molecular mechanism for the generation of ligand-dependent differential outputs by the epidermal growth factor receptor. ELife, 2021, 10, .	2.8	44
11	Structural analysis of receptor binding domain mutations in SARS-CoV-2 variants of concern that modulate ACE2 and antibody binding. Cell Reports, 2021, 37, 110156.	2.9	67
12	High Potency of a Bivalent Human VH Domain in SARS-CoV-2 Animal Models. Cell, 2020, 183, 429-441.e16.	13.5	100
13	Host membrane lipids are trafficked to membranes of intravacuolar bacterium <i>Ehrlichia chaffeensis</i> . Proceedings of the National Academy of Sciences of the United States of America, 2020, 117, 8032-8043.	3.3	20
14	Biochemical and structural analyses reveal that the tumor suppressor neurofibromin (NF1) forms a high-affinity dimer. Journal of Biological Chemistry, 2020, 295, 1105-1119.	1.6	25
15	<i>Plasmodium vivax</i> and human hexokinases share similar active sites but display distinct quaternary architectures. IUCrJ, 2020, 7, 453-461.	1.0	6
16	1.8 à resolution structure of β-galactosidase with a 200â€kV CRYO ARM electron microscope. IUCrJ, 2020, 7, 639-643.	1.0	26
17	COVID-19 and cryo-EM. IUCrJ, 2020, 7, 575-576.	1.0	9
18	Cryo-EM structures reveal coordinated domain motions that govern DNA cleavage by Cas9. Nature Structural and Molecular Biology, 2019, 26, 679-685.	3.6	97

SRIRAM SUBRAMANIAM

#	Article	IF	CITATIONS
19	Structure of the primed state of the ATPase domain of chromatin remodeling factor ISWI bound to the nucleosome. Nucleic Acids Research, 2019, 47, 9400-9409.	6.5	30
20	Cryo-EM structure of a dimeric B-Raf:14-3-3 complex reveals asymmetry in the active sites of B-Raf kinases. Science, 2019, 366, 109-115.	6.0	127
21	Frontiers in Cryo Electron Microscopy of Complex Macromolecular Assemblies. Annual Review of Biomedical Engineering, 2019, 21, 395-415.	5.7	44
22	Semi-automated 3D segmentation of human skeletal muscle using Focused Ion Beam-Scanning Electron Microscopic images. Journal of Structural Biology, 2019, 207, 1-11.	1.3	18
23	The cryo-EM revolution: fueling the next phase. IUCrJ, 2019, 6, 1-2.	1.0	32
24	A Tail-Based Mechanism Drives Nucleosome Demethylation by the LSD2/NPAC Multimeric Complex. Cell Reports, 2019, 27, 387-399.e7.	2.9	31
25	Cryo-electron microscopy instrumentation and techniques for life sciences and materials science. MRS Bulletin, 2019, 44, 929-934.	1.7	7
26	Deep-Learning-Assisted Volume Visualization. IEEE Transactions on Visualization and Computer Graphics, 2019, 25, 1378-1391.	2.9	24
27	Microbiology catches the cryo-EM bug. Current Opinion in Microbiology, 2018, 43, 199-207.	2.3	9
28	Structural mechanisms of centromeric nucleosome recognition by the kinetochore protein CENP-N. Science, 2018, 359, 339-343.	6.0	98
29	Atomic Resolution Cryo-EM Structure of Î ² -Galactosidase. Structure, 2018, 26, 848-856.e3.	1.6	115
30	Cryo-EM structure of human rhodopsin bound to an inhibitory G protein. Nature, 2018, 558, 553-558.	13.7	230
31	Single-particle cryo-EM structure of a voltage-activated potassium channel in lipid nanodiscs. ELife, 2018, 7, .	2.8	80
32	Power Grid Protection of the Muscle Mitochondrial Reticulum. Cell Reports, 2017, 19, 487-496.	2.9	155
33	Cryo-EM Structures Reveal Mechanism and Inhibition of DNA Targeting by a CRISPR-Cas Surveillance Complex. Cell, 2017, 171, 414-426.e12.	13.5	158
34	Broadly protective murine monoclonal antibodies against influenza B virus target highly conserved neuraminidase epitopes. Nature Microbiology, 2017, 2, 1415-1424.	5.9	96
35	Cryo-EM: beyond the microscope. Current Opinion in Structural Biology, 2017, 46, 71-78.	2.6	76
36	CryoEM at IUCrJ : a new era. IUCrJ, 2016, 3, 3-7.	1.0	54

3

#	Article	IF	CITATIONS
37	Mapping of Ebolavirus Neutralization by Monoclonal Antibodies in the ZMapp Cocktail Using Cryo-Electron Tomography and Studies of Cellular Entry. Journal of Virology, 2016, 90, 7618-7627.	1.5	32
38	Structural basis for early-onset neurological disorders caused by mutations in human selenocysteine synthase. Scientific Reports, 2016, 6, 32563.	1.6	13
39	Cryo-electron Microscopy Structures of Chimeric Hemagglutinin Displayed on a Universal Influenza Vaccine Candidate. MBio, 2016, 7, e00257.	1.8	26
40	Breaking Cryo-EM Resolution Barriers to Facilitate Drug Discovery. Cell, 2016, 165, 1698-1707.	13.5	458
41	Cryo-EM Analysis of the Conformational Landscape of Human P-glycoprotein (ABCB1) During its Catalytic Cycle. Molecular Pharmacology, 2016, 90, 35-41.	1.0	75
42	The crystal structure of human GlnRS provides basis for the development of neurological disorders. Nucleic Acids Research, 2016, 44, 3420-3431.	6.5	14
43	Using Cryo-EM to Map Small Ligands on Dynamic Metabolic Enzymes: Studies with Glutamate Dehydrogenase. Molecular Pharmacology, 2016, 89, 645-651.	1.0	41
44	Cryo-EM of viruses and vaccine design. Proceedings of the National Academy of Sciences of the United States of America, 2016, 113, 8903-8905.	3.3	16
45	The democratization of cryo-EM. Nature Methods, 2016, 13, 607-608.	9.0	35
46	Resolution advances in cryo-EM enable application to drug discovery. Current Opinion in Structural Biology, 2016, 41, 194-202.	2.6	95
47	Structural basis of kainate subtype glutamate receptor desensitization. Nature, 2016, 537, 567-571.	13.7	78
48	2.3 Ã resolution cryo-EM structure of human p97 and mechanism of allosteric inhibition. Science, 2016, 351, 871-875.	6.0	305
49	Cryo-EM Structures of the Magnesium Channel CorA Reveal Symmetry Break upon Gating. Cell, 2016, 164, 747-756.	13.5	111
50	A versatile nano display platform from bacterial spore coat proteins. Nature Communications, 2015, 6, 6777.	5.8	35
51	Griffithsin tandemers: flexible and potent lectin inhibitors of the human immunodeficiency virus. Retrovirology, 2015, 12, 6.	0.9	34
52	Maturation of the HIV-1 core by a non-diffusional phase transition. Nature Communications, 2015, 6, 5854.	5.8	49
53	Mitochondrial reticulum for cellular energy distribution in muscle. Nature, 2015, 523, 617-620.	13.7	355
54	Cryo-EM structure of the bacteriophage T4 portal protein assembly at near-atomic resolution. Nature Communications, 2015, 6, 7548.	5.8	88

#	Article	IF	CITATIONS
55	2.2 à resolution cryo-EM structure of β-galactosidase in complex with a cell-permeant inhibitor. Science, 2015, 348, 1147-1151.	6.0	440
56	Focused ion beams in biology. Nature Methods, 2015, 12, 1021-1031.	9.0	184
57	Three-Dimensional Imaging of HIV-1 Virological Synapses Reveals Membrane Architectures Involved in Virus Transmission. Journal of Virology, 2014, 88, 10327-10339.	1.5	61
58	A 3D cellular context for the macromolecular world. Nature Structural and Molecular Biology, 2014, 21, 841-845.	3.6	47
59	Spatial Localization of the Ebola Virus Glycoprotein Mucin-Like Domain Determined by Cryo-Electron Tomography. Journal of Virology, 2014, 88, 10958-10962.	1.5	53
60	Structure of β-galactosidase at 3.2-à resolution obtained by cryo-electron microscopy. Proceedings of the United States of America, 2014, 111, 11709-11714.	3.3	184
61	Multi-resolution correlative focused ion beam scanning electron microscopy: Applications to cell biology. Journal of Structural Biology, 2014, 185, 278-284.	1.3	99
62	Three-Dimensional Imaging of Viral Infections. Annual Review of Virology, 2014, 1, 453-473.	3.0	49
63	Structural mechanism of glutamate receptor activation and desensitization. Nature, 2014, 514, 328-334.	13.7	207
64	Single-Particle Cryo-Electron Microscopy (Cryo-EM). Advances in Imaging and Electron Physics, 2014, , 113-137.	0.1	20
65	Accelerating Discovery in 3D Microanalysis: Leveraging Open Source Software and Deskside High Performance Computing. Microscopy and Microanalysis, 2014, 20, 774-775.	0.2	0
66	Self-assembled monolayers improve protein distribution on holey carbon cryo-EM supports. Scientific Reports, 2014, 4, 7084.	1.6	88
67	Targeted conformational search with map-restrained self-guided Langevin dynamics: Application to flexible fitting into electron microscopic density maps. Journal of Structural Biology, 2013, 183, 429-440.	1.3	50
68	HIV-1 envelope glycoprotein structure. Current Opinion in Structural Biology, 2013, 23, 268-276.	2.6	73
69	Cryoâ€electron microscopy – a primer for the nonâ€microscopist. FEBS Journal, 2013, 280, 28-45.	2.2	194
70	A collaborative framework for 3D alignment and classification of heterogeneous subvolumes in cryo-electron tomography. Journal of Structural Biology, 2013, 181, 116-127.	1.3	524
71	Catching HIV â€`in the act' with 3D electron microscopy. Trends in Microbiology, 2013, 21, 397-404.	3.5	21
72	Prefusion structure of trimeric HIV-1 envelope glycoprotein determined by cryo-electron microscopy. Nature Structural and Molecular Biology, 2013, 20, 1352-1357.	3.6	152

#	Article	lF	CITATIONS
73	HIV-1 Envelope Glycoprotein Trimers Display Open Quaternary Conformation When Bound to the gp41 Membrane-Proximal External-Region-Directed Broadly Neutralizing Antibody Z13e1. Journal of Virology, 2013, 87, 7191-7196.	1.5	27
74	Molecular structures of trimeric HIV-1 Env in complex with small antibody derivatives. Proceedings of the United States of America, 2013, 110, 513-518.	3.3	44
75	Glutamate receptor desensitization is mediated by changes in quaternary structure of the ligand binding domain. Proceedings of the National Academy of Sciences of the United States of America, 2013, 110, 5921-5926.	3.3	53
76	Structure and accessibility of HA trimers on intact 2009 H1N1 pandemic influenza virus to stem region-specific neutralizing antibodies. Proceedings of the National Academy of Sciences of the United States of America, 2013, 110, 4592-4597.	3.3	99
77	Structure of trimeric HIV-1 envelope glycoproteins. Proceedings of the National Academy of Sciences of the United States of America, 2013, 110, E4172-4.	3.3	39
78	Complexes of Neutralizing and Non-Neutralizing Affinity Matured Fabs with a Mimetic of the Internal Trimeric Coiled-Coil of HIV-1 gp41. PLoS ONE, 2013, 8, e78187.	1.1	17
79	Derivation of Neural Stem Cells from Human Adult Peripheral CD34+ Cells for an Autologous Model of Neuroinflammation. PLoS ONE, 2013, 8, e81720.	1.1	26
80	Structural Mechanism of Trimeric HIV-1 Envelope Glycoprotein Activation. PLoS Pathogens, 2012, 8, e1002797.	2.1	182
81	Data management challenges in three-dimensional EM. Nature Structural and Molecular Biology, 2012, 19, 1203-1207.	3.6	49
82	Shape-Based Regularization of Electron Tomographic Reconstruction. IEEE Transactions on Medical Imaging, 2012, 31, 2241-2252.	5.4	10
83	Chemical mapping of mammalian cells by atom probe tomography. Journal of Structural Biology, 2012, 178, 98-107.	1.3	41
84	Computational separation of conformational heterogeneity using cryo-electron tomography and 3D sub-volume averaging. Journal of Structural Biology, 2012, 178, 165-176.	1.3	19
85	Protein Secondary Structure Determination by Constrained Single-Particle Cryo-Electron Tomography. Structure, 2012, 20, 2003-2013.	1.6	90
86	There is no overkill in biochemistry. Resonance, 2012, 17, 1157-1164.	0.2	0
87	Visualizing Cells and Humans in 3D: Biomedical Image Analysis at Nanometer and Meter Scales. IEEE Computer Graphics and Applications, 2012, 32, 39-49.	1.0	4
88	Structural plasticity of a transmembrane peptide allows self-assembly into biologically active nanoparticles. Proceedings of the National Academy of Sciences of the United States of America, 2011, 108, 9798-9803.	3.3	45
89	Compositional Mapping of the Surface and Interior of Mammalian Cells at Submicrometer Resolution. Analytical Chemistry, 2011, 83, 1207-1213.	3.2	42
90	Correlative 3D imaging of whole mammalian cells with light and electron microscopy. Journal of Structural Biology, 2011, 176, 268-278.	1.3	81

#	Article	IF	CITATIONS
91	HIV-1 activates Cdc42 and induces membrane extensions in immature dendritic cells to facilitate cell-to-cell virus propagation. Blood, 2011, 118, 4841-4852.	0.6	79
92	Determination of Molecular Structures of HIV Envelope Glycoproteins using Cryo-Electron Tomography and Automated Sub-tomogram Averaging. Journal of Visualized Experiments, 2011, , .	0.2	14
93	Chemotaxis kinase CheA is activated by three neighbouring chemoreceptor dimers as effectively as by receptor clusters. Molecular Microbiology, 2011, 79, 677-685.	1.2	38
94	Lateral density of receptor arrays in the membrane plane influences sensitivity of the E. coli chemotaxis response. EMBO Journal, 2011, 30, 1719-1729.	3.5	37
95	Three-Dimensional Structures of Soluble CD4-Bound States of Trimeric Simian Immunodeficiency Virus Envelope Glycoproteins Determined by Using Cryo-Electron Tomography. Journal of Virology, 2011, 85, 12114-12123.	1.5	46
96	Spiral Architecture of the Nucleoid in <i>Bdellovibrio bacteriovorus</i> . Journal of Bacteriology, 2011, 193, 1341-1350.	1.0	47
97	Trimeric HIV-1 glycoprotein gp140 immunogens and native HIV-1 envelope glycoproteins display the same closed and open quaternary molecular architectures. Proceedings of the National Academy of Sciences of the United States of America, 2011, 108, 11440-11445.	3.3	149
98	A coiled-coil-repeat protein â€~Ccrp' in Bdellovibrio bacteriovorus prevents cellular indentation, but is not essential for vibroid cell morphology. FEMS Microbiology Letters, 2010, 313, 89-95.	0.7	11
99	3D visualization of HIV transfer at the virological synapse between dendritic cells and T cells. Proceedings of the National Academy of Sciences of the United States of America, 2010, 107, 13336-13341.	3.3	169
100	Molecular Architectures of Trimeric SIV and HIV-1 Envelope Glycoproteins on Intact Viruses: Strain-Dependent Variation in Quaternary Structure. PLoS Pathogens, 2010, 6, e1001249.	2.1	161
101	Ion-abrasion scanning electron microscopy reveals distorted liver mitochondrial morphology in murine methylmalonic acidemia. Journal of Structural Biology, 2010, 171, 125-132.	1.3	31
102	Protein Conformational Changes in the Bacteriorhodopsin Photocycle: Comparison of Findings from Electron and X-Ray Crystallographic Analyses. PLoS ONE, 2009, 4, e5769.	1.1	38
103	Ion-Abrasion Scanning Electron Microscopy Reveals Surface-Connected Tubular Conduits in HIV-Infected Macrophages. PLoS Pathogens, 2009, 5, e1000591.	2.1	151
104	Membrane protein structure determination using cryo-electron tomography and 3D image averaging. Current Opinion in Structural Biology, 2009, 19, 402-407.	2.6	65
105	Structural snapshots of conformational changes in a seven-helix membrane protein: lessons from bacteriorhodopsin. Current Opinion in Structural Biology, 2009, 19, 433-439.	2.6	64
106	Cryo-electron tomography of bacteria: progress, challenges and future prospects. Nature Reviews Microbiology, 2009, 7, 666-675.	13.6	144
107	Automatic joint classification and segmentation of whole cell 3D images. Pattern Recognition, 2009, 42, 1067-1079.	5.1	42
108	3D Imaging of mammalian cells with ion-abrasion scanning electron microscopy. Journal of Structural Biology, 2009, 166, 1-7.	1.3	113

7

SRIRAM SUBRAMANIAM

#	Article	IF	CITATIONS
109	3D imaging of diatoms with ion-abrasion scanning electron microscopy. Journal of Structural Biology, 2009, 166, 316-328.	1.3	71
110	Staphylococcal Enterotoxin A Induces Small Clusters of HLA-DR1 on B Cells. PLoS ONE, 2009, 4, e6188.	1.1	5
111	Molecular architecture of native HIV-1 gp120 trimers. Nature, 2008, 455, 109-113.	13.7	720
112	Extended Polypeptide Linkers Establish the Spatial Architecture of a Pyruvate Dehydrogenase Multienzyme Complex. Structure, 2008, 16, 93-103.	1.6	22
113	Evaluation of denoising algorithms for biological electron tomography. Journal of Structural Biology, 2008, 164, 7-17.	1.3	38
114	Three-Dimensional Imaging of the Highly Bent Architecture of <i>Bdellovibrio bacteriovorus</i> by Using Cryo-Electron Tomography. Journal of Bacteriology, 2008, 190, 2588-2596.	1.0	55
115	Chemoreceptors in <i>Caulobacter crescentus</i> : Trimers of Receptor Dimers in a Partially Ordered Hexagonally Packed Array. Journal of Bacteriology, 2008, 190, 6805-6810.	1.0	72
116	Electron tomography in nanoparticle imaging and analysis. Nanomedicine, 2008, 3, 125-131.	1.7	70
117	Role of HAMP domains in chemotaxis signaling by bacterial chemoreceptors. Proceedings of the National Academy of Sciences of the United States of America, 2008, 105, 16555-16560.	3.3	72
118	Stoichiometry and Absolute Quantification of Proteins with Mass Spectrometry Using Fluorescent and Isotope-labeled Concatenated Peptide Standards. Molecular and Cellular Proteomics, 2008, 7, 442-447.	2.5	42
119	Cell Surface Filaments of the Gliding Bacterium <i>Flavobacterium johnsoniae</i> Revealed by Cryo-Electron Tomography. Journal of Bacteriology, 2007, 189, 7503-7506.	1.0	76
120	Direct visualization of Escherichia coli chemotaxis receptor arrays using cryo-electron microscopy. Proceedings of the National Academy of Sciences of the United States of America, 2007, 104, 3777-3781.	3.3	176
121	Cryoelectron Tomographic Analysis of an HIV-neutralizing Protein and Its Complex with Native Viral gp120*. Journal of Biological Chemistry, 2007, 282, 27754-27759.	1.6	35
122	FROM GIGABYTES TO BYTES: AUTOMATED DENOISING AND FEATURE IDENTIFICATION IN ELECTRON TOMOGRAMS OF INTACT BACTERIAL CELLS. , 2007, , .		1
123	Electron Tomography of the Contact between T Cells and SIV/HIV-1: Implications for Viral Entry. PLoS Pathogens, 2007, 3, e63.	2.1	165
124	Gigabytes to Bytes: Automated Denoising and Feature Extraction as Applied to the Analysis of HIV Architecture and Variability using Electron Tomography. , 2007, , .		0
125	Electron Tomography of Bacterial Chemotaxis Receptor Assemblies. Methods in Cell Biology, 2007, 79, 373-384.	0.5	9
126	DETERMINATION OF PROTEIN STRUCTURES IN SITU: ELECTRON TOMOGRAPHY OF INTACT VIRUSES AND CELLS. , 2007, , .		0

SRIRAM SUBRAMANIAM

#	Article	IF	CITATIONS
127	Automated 100-position specimen loader and image acquisition system for transmission electron microscopy. Journal of Structural Biology, 2007, 158, 318-326.	1.3	30
128	Electron tomography of viruses. Current Opinion in Structural Biology, 2007, 17, 596-602.	2.6	54
129	Site-specific 3D imaging of cells and tissues with a dual beam microscope. Journal of Structural Biology, 2006, 155, 63-73.	1.3	311
130	The SIV Surface Spike Imaged by Electron Tomography: One Leg or Three?. PLoS Pathogens, 2006, 2, e91.	2.1	21
131	Molecular Structure of a 9-MDa Icosahedral Pyruvate Dehydrogenase Subcomplex Containing the E2 and E3 Enzymes Using Cryoelectron Microscopy. Journal of Biological Chemistry, 2006, 281, 4364-4370.	1.6	72
132	Bridging the imaging gap in nanobiology with three-dimensional electron microscopy. , 2006, , .		0
133	An energy-based three-dimensional segmentation approach for the quantitative interpretation of electron tomograms. IEEE Transactions on Image Processing, 2005, 14, 1314-1323.	6.0	38
134	Bridging the imaging gap: visualizing subcellular architecture with electron tomography. Current Opinion in Microbiology, 2005, 8, 316-322.	2.3	68
135	Electron tomography of degenerating neurons in mice with abnormal regulation of iron metabolism. Journal of Structural Biology, 2005, 150, 144-153.	1.3	55
136	Three-Dimensional Electron Microscopy at Molecular Resolution. Annual Review of Biophysics and Biomolecular Structure, 2004, 33, 141-155.	18.3	65
137	Three-Dimensional Electron Microscopic Imaging of Membrane Invaginations in Escherichia coli Overproducing the Chemotaxis Receptor Tsr. Journal of Bacteriology, 2004, 186, 5052-5061.	1.0	70
138	Structure and Transport Mechanism of the Bacterial Oxalate Transporter OxlT. Biophysical Journal, 2004, 87, 3600-3607.	0.2	59
139	Site-specific 3D Imaging of Cells and Tissues Using DualBeam Technology. Microscopy and Microanalysis, 2004, 10, 1124-1125.	0.2	7
140	Projection structure of the bacterial oxalate transporter OxlT at 3.4Ã resolution. Journal of Structural Biology, 2003, 144, 320-326.	1.3	25
141	Structural insights into the mechanism of proton pumping by bacteriorhodopsin. FEBS Letters, 2003, 545, 2-8.	1.3	35
142	A core-weighted fitting method for docking atomic structures into low-resolution maps: Application to cryo-electron microscopy. Journal of Structural Biology, 2003, 141, 63-76.	1.3	77
143	Automated image acquisition and processing using a new generation of 4K×4K CCD cameras for cryo electron microscopic studies of macromolecular assemblies. Journal of Structural Biology, 2003, 143, 135-144.	1.3	57
144	Electron Microscopic Analysis of Membrane Assemblies Formed by the Bacterial Chemotaxis Receptor Tsr. Journal of Bacteriology, 2003, 185, 3636-3643.	1.0	62

#	Article	IF	CITATIONS
145	Structural Model for 12-Helix Transporters Belonging to the Major Facilitator Superfamily. Journal of Bacteriology, 2003, 185, 1712-1718.	1.0	103
146	The Pyruvate Dehydrogenase Multienzyme Complex. Oxidative Stress and Disease, 2003, , .	0.3	0
147	From structure to mechanism: electron crystallographic studies of bacteriorhodopsin. Philosophical Transactions Series A, Mathematical, Physical, and Engineering Sciences, 2002, 360, 859-874.	1.6	36
148	Molecular Structure of an Icosahedral Pyruvate Dehydrogenase Complex. Microscopy and Microanalysis, 2002, 8, 214-215.	0.2	0
149	Three-dimensional structure of a bacterial oxalate transporter. Nature Structural Biology, 2002, 9, 597-600.	9.7	114
150	Molecular architecture and mechanism of an icosahedral pyruvate dehydrogenase complex: a multifunctional catalytic machine. EMBO Journal, 2002, 21, 5587-5598.	3.5	115
151	Automated Data Collection with a Tecnai 12 Electron Microscope: Applications for Molecular Imaging by Cryomicroscopy. Journal of Structural Biology, 2001, 135, 251-261.	1.3	47
152	CCD detectors in high-resolution biological electron microscopy. Quarterly Reviews of Biophysics, 2000, 33, 1-27.	2.4	61
153	Molecular mechanism of vectorial proton translocation by bacteriorhodopsin. Nature, 2000, 406, 653-657.	13.7	451
154	Crystallographic analysis of protein conformational changes in the bacteriorhodopsin photocycle. Biochimica Et Biophysica Acta - Bioenergetics, 2000, 1460, 157-165.	0.5	44
155	The structure of bacteriorhodopsin: an emerging consensus. Current Opinion in Structural Biology, 1999, 9, 462-468.	2.6	45
156	Protein conformational changes in the bacteriorhodopsin photocycle 1 1Edited by B. Honig. Journal of Molecular Biology, 1999, 287, 145-161.	2.0	244
157	Electron Crystallography of Bacteriorhodopsin with Millisecond Time Resolution. Journal of Structural Biology, 1999, 128, 19-25.	1.3	49
158	Studies of Rh1 Metarhodopsin Stabilization in Wild-TypeDrosophilaand in Mutants Lacking One or Both Arrestinsâ€. Biochemistry, 1997, 36, 2188-2196.	1.2	16
159	Expression of bacteriorhodopsin in Sf9 and COS-1 cells. Journal of Bioenergetics and Biomembranes, 1997, 29, 55-59.	1.0	4
160	Modulation of Arrestin Release in the Light-Driven Regeneration of Rh1DrosophilaRhodopsinâ€. Biochemistry, 1996, 35, 1848-1855.	1.2	9
161	Critical mixing in monolayer mixtures of phospholipid and cholesterol. The Journal of Physical Chemistry, 1987, 91, 1715-1718.	2.9	132
162	Mono- and bilayers of phospholipids at interfaces: interlayer coupling and phase stability. The Journal of Physical Chemistry, 1985, 89, 3592-3595.	2.9	48